Optics Letters

Heterogeneous integration of GaInAsSb–GaSb photodiodes on SOI photonic integrated circuits for SWIR applications

XIN GUO,[1,2,*] LAURENT CERUTTI,[3] JEAN-BATISTE RODRIGUEZ,[3] ERIC TOURNIÉ,[3] SARAH UVIN,[1,2] AND GUNTHER ROELKENS[1,2]

[1] *Photonics Research Group, Department of Information Technology, Ghent University-imec, Ghent 9052, Belgium*
[2] *Center for Nano- and Biophotonics, Ghent University, Ghent 9052, Belgium*
[3] *Institut d'Electronique du Sud (IES), UMR 5214 Université Montpellier 2 – CNRS, Montpellier cedex 5 F-34095, France*
**Xin.Guo@UGent.be*

Received 2 October 2024; revised 20 November 2024; accepted 7 December 2024; posted 9 December 2024; published 17 December 2024

We demonstrate the heterogeneous integration of GaInAsSb–GaSb photodiodes on 220 nm SOI photonic integrated circuits (PICs) using the micro-transfer-printing (μTP) technology, for operation in the short-wave infrared (SWIR) wavelength region. Utilizing an evanescent coupling scheme between a silicon waveguide and a III–V structure, the device exhibits a room temperature responsivity of 1.23 and 1.25 A/W at 2.3 and 2.45 μm, respectively. This enables the realization of photonic integrated circuits for SWIR applications. © 2024 Optica Publishing Group. All rights, including for text and data mining (TDM), Artificial Intelligence (AI) training, and similar technologies, are reserved.

https://doi.org/10.1364/OL.543948

Introduction. In the last two decades, silicon photonics (SiPh) has become an established platform for realizing telecommunication and data communication transceivers. Recently, with the exploration of opportunities beyond traditional telecom wavelengths, numerous potential applications for the photonic integrated circuit (PIC) technology have emerged. For example, the short-wave infrared (SWIR) wavelength range and especially the 2–2.5 μm range are of particular interest for spectroscopic sensing applications [1,2]. Various molecules, including carbon dioxide (e.g., CO_2, NH_3, and CH_4), glucose, lactate, urea, and ethanol, have absorption peaks in this spectral region, enabling environmental monitoring and medical diagnostics. While silicon photonic passive waveguide circuits are known to operate in the 2–2.5 μm wavelength range, the platform lacks efficient photodiodes in this wavelength range, as Ge has a cut-off wavelength of around 1600 nm. Various approaches have been studied to realize photodetection in the SWIR on a silicon PIC. Table 1 shows a comparison of the state-of-the-art waveguide-coupled photodiodes operating at 2–2.5 μm. Common methods include flip-chip integration and die-to-wafer bonding, typically using InP- or GaSb-based devices/materials [3–7]. These approaches, however, require relatively large III–V dies and large-area planarized surfaces on the target wafer. Emerging research fields such as two-dimensional (2D) materials (graphene, black phosphorus) or colloidal quantum dots for on-chip photodetection at these wavelengths show promising properties but often require specific process steps, making them challenging to scale up and industrialize [8–11]. Furthermore, cost-effective photodiodes on silicon, achieved by directly growing GeSn alloys [12,13] or III–V quantum dots [14], often result in high dark currents due to the lattice mismatch with silicon. Micro-transfer printing (μTP) is a versatile technology that allows efficient integration of III–V materials on silicon photonics [15]. It allows separate pre-processing and testing of the devices that need to be integrated on the photonic integrated circuit. This technology allows the efficient use of III–V materials and integration of a wide range of materials/devices on a wafer scale in a massively parallel way. Several demonstrations have been made on C-band photodiodes using μTP, based on group IV or III–V materials [16–18]. In this work, we report, for the first time, the μTP integration of GaSb-based photodiodes operating up to 2.45 μm on a 220 nm silicon photonic platform. We demonstrate a responsivity of 1.25 A/W at 2.45 μm via evanescent coupling, at a bias of −0.3 V, with a dark current of 3 μA at room temperature.

Design and simulation. Antimony (Sb)-based materials are employed for photodetection in the short-wave infrared (SWIR) and mid-wave infrared (MWIR) ranges. This material system can incorporate two group V elements (Sb and As) and three group III elements (Ga, In, and Al), allowing it to cover the entire SWIR/MWIR spectrum and achieve lattice matching with GaSb or InAs substrates. In this work, the design of the epitaxial layer stack (see Table 2) is based on the work in [5]. The intrinsic absorption region consists of a not intentionally doped 800 nm thick $Ga_{0.79}In_{0.21}As_{0.19}Sb_{0.81}$ layer. This layer is surrounded by two 100 nm GaInAsSb and GaSb layers, with n and p doping, respectively. The n-GaSb layer is 350 nm thick and the p-layer is 500 nm. To make the device μTP compatible, a 1500 nm InAsSb release layer is added between the functional layers and the GaSb substrate. This layer allows the photodiodes to be released from the GaSb substrate using selective etchant(s). The SOI waveguide circuit consists of 220 nm thick silicon waveguides on top of a 2 μm buried oxide layer. The waveguides are fully etched and are 900 nm wide, which is covered by 170 nm

Table 1. State of the Art of Waveguide-Coupled Photodiodes at 2–2.5 μm

Material	Wavelength (μm)	R (A/W)	Dark Current (Density)	Dimension of Device (μm)	Ref
GaInAsSb–GaSb	2.3	1.4	0.3 A/cm^2 at −1 V	60 × 10	[3–5]
InP	2.35	1.6	10 nA at −0.5 V	150 × 3.5	[6,7]
Graphene	2.05	0.25	\	\	[11]
GeSn	2.36	1.55	\	3000 × 10	[12,13]
Colloidal quantum dot	2.1	1.3	0.1 A/cm^2 at −0.5 V	200 × 30	[10]
GaInAsSb–GaSb (this work)	2.3/2.45	1.23/1.25	0.52 A/cm^2 at −0.3 V	28 × 28	

Table 2. Epitaxial Layer Stack of the GaSb Photodiode

Feature	Material	T (nm)	Doping (cm^{-3})
p contact	GaSb	500	p = 1 × 10^{19}
p-layer	GaInAsSb	100	p = 1 × 10^{18}
Absorption region	GaInAsSb	800	n.i.d.
n-layer	GaInAsSb	100	n = 1 × 10^{18}
n contact	GaSb	350	n = 3 × 10^{18}
Release layer	InAsSb	1500	n.i.d.
Substrate	GaSb	–	n = 1 × 10^{18}

silicon dioxide. There is a about 50 nm DVS-BCB:mesitylene (BCB) as the bonding layer for μTP. Optical simulation is carried out in Lumerical FDTD to find out the optimal length of the photodiode. Figure 1(a) shows the field plot for the evanescently coupling scheme with the complete photodiode structure, including a 500 nm gold metal layer on top. Part of the light is not absorbed in the absorption region but gets absorbed by the metal layer, limiting the total absorption to 84%. A sweep of the absorption as a function of the length of simulation is performed (Fig. 1(b)), showing that a 25–30 μm device length is sufficient.

Fabrication. The GaSb photodiodes are patterned on the native GaSb wafer (Figs. 2(a)–2(c)). The p-mesa has a width of 4 μm and the whole absorption region is 28 × 28 μm. Four hundred nanometer SiNx is deposited as the passivation before the metal deposition. A 3 μm wide opening is etched down to expose the contact layer. A Ti/Pt/Au metal stack is used for both n- and p-type contacts. To make the devices transfer-printable, these diodes are further processed. Firstly, the release layer is being patterned with a padding of a few μm around the diode. A 600 nm SiNx layer is deposited and patterned to form tethers, which will hold the device in place during the release etch while leaving the metal areas exposed. Additional photoresist is applied to planarize the coupon. The release layer is then selectively etched using a mixture of citric acid and hydrogen peroxide (2:1 v/v) at 65°C. At this point, the coupons are released and held by the SiNx tethers (Fig. 2(d)). The μTP process is enabled by an X-Celeprint TP-100 tool. To transfer-print these coupons onto the target PIC chip, a dedicated PDMS stamp with the same dimension as the coupon is used. The flexible PDMS stamp picks up the coupon from the source wafer by retracting the stamp, and by laminating the stamp onto the target wafer, the coupon is successfully printed. To ensure a high printing yield, a DVS-BCB:mesitylene layer is spin-coated on the target sample (1:5 solution at 3000 rpm) and then soft baked at 150°C for 10 min. This bonding material will eventually form a 10–30 nm bonding layer between the III–V coupon and the silicon waveguide. Finally, the protective photoresist is removed and additional metallization is applied to enable wire-bonding or probing (Fig. 2(f)) on the target wafer. A picture of a fully processed transfer-printed photodiode and a focused-ion-beam (FIB) image of the cross section of the diode are shown in Fig. 3.

Experimental results. *Passive circuit*. The SOI waveguide circuit consists of 220 nm thick silicon waveguides on top of a 2 μm buried oxide layer. The waveguides are fully etched and are 900 nm wide. Such waveguides are tested to have a loss of around 1 dB/cm for TE polarization [19]. The waveguide is covered by 170 nm silicon dioxide. The grating coupler (grating period of 1350 nm, fill factor 0.5, and etch depth 160 nm) is designed for the 2200–2500 nm wavelength range, showing a measured loss of 8.2 dB at 2.3 μm and 9.2 dB at 2.45 μm, with fiber injection angles at 20 and 10°, respectively.

Dark current. The I–V characteristics of our 28 × 28 μm photodiodes were measured at different temperatures, as shown in Fig. 4. At room temperature, we measured a dark current of 3 μA at a bias of −0.3 V, which corresponds to a dark current density of 0.52 A/cm^2. We attribute the majority of the dark current to surface leakage current originating from the mesa sidewalls. As expected, the dark current increases with temperature, remaining below 20 μA at −0.3 V bias even at 68°C.

This trade-off is particularly tolerable given that this is the first demonstration of a transfer-printed photodiode. While the dark current density is slightly higher than that of photodiodes

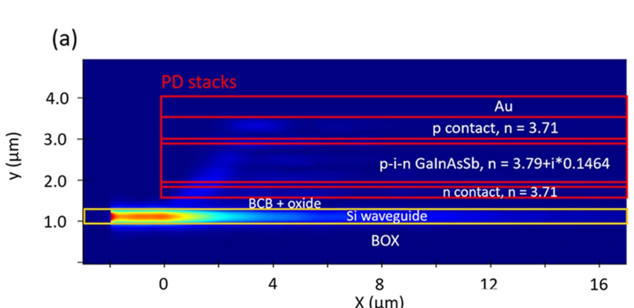

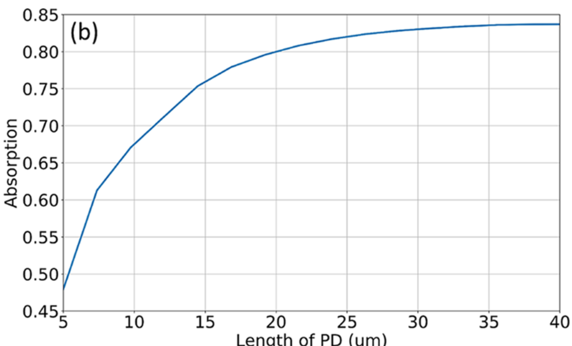

Fig. 1. Optical coupling simulation at 2.3 μm (TE polarization). (a) Light propagation in the evanescently coupled PD structure. (b) Device absorption as a function of photodiode length.

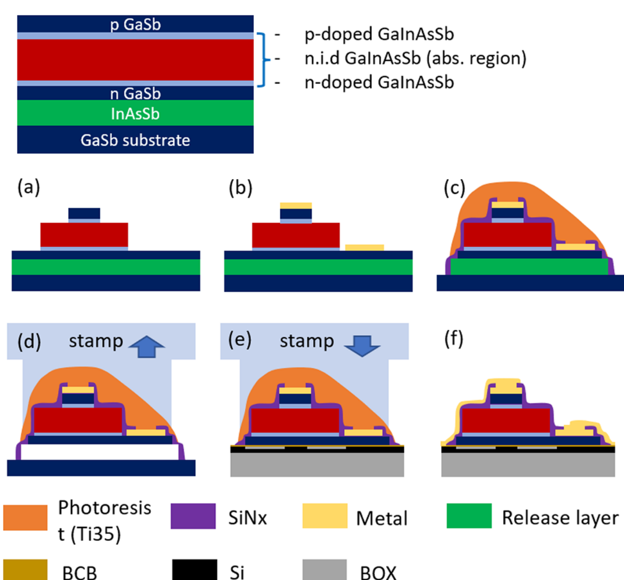

Fig. 2. Schematic of a process flow. (a) Patterning the diode by etching the mesa. (b) Deposition of p and n contacts. (c) Patterning of the release layer and applying a tether before release etch (with metal being opened). (d) Wet etching on the release layer and pick up the coupon. (e) Printing of the coupon on a SOI circuit. (f) Final metallization on a transfer-printed device.

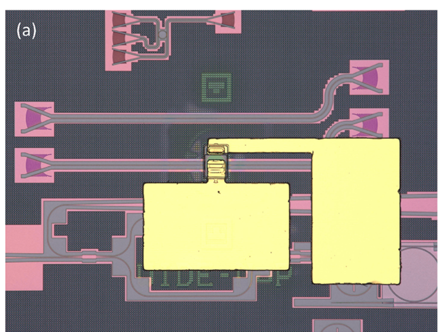

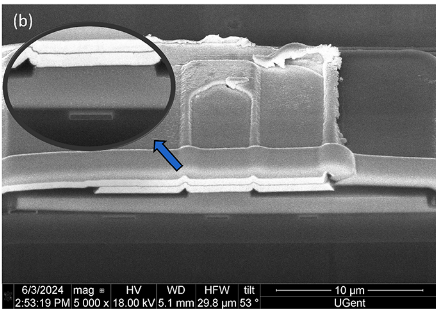

Fig. 3. Images of the GaSb photodiodes on SOI. (a) Microscope picture of the device after final metallization. (b) Cross-sectional FIB image of the diode and silicon waveguide.

fabricated using bonding methods, the observed performance remains within the same order of magnitude.

Responsivity and linearity. The responsivity of the photodiodes is measured at a wavelength of 2.3 and 2.45 μm (Fig. 5), using a single-frequency tunable Cr:ZnS/Se laser source from IPG Photonics. A Thorlabs portable powermeter is used for

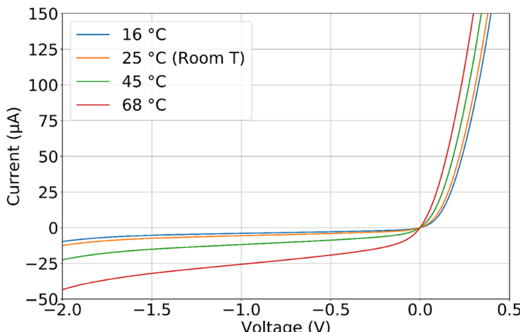

Fig. 4. Photodiode dark current dependence on temperature.

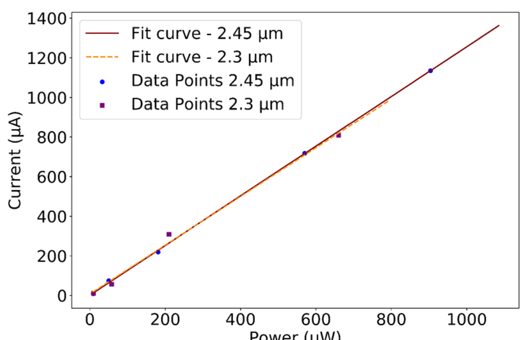

Fig. 5. Photocurrent versus input power at 2.3 and 2.45 μm, at −0.3 V bias.

measuring the laser output power. At 2.3 μm, the device shows a responsivity of 1.23 A/W under −0.3 V bias at room temperature. This results in a waveguide-referred quantum efficiency (WQE) of 65%. The responsivity increases to 1.25 A/W at 2.45 μm, corresponding to a WQE of 62%. The slight drop of the WQE value is expected since 2.45 μm is close to the cut-off wavelength of the designed epitaxial layer stack. The linearity of the device is also featured in Fig. 5.

Conclusion. For the first time, a waveguide-evanescent-coupled GaSb-based photodiode is integrated on a silicon photonic platform by μTP. This novel approach allow us to fabricate the III–V active coupon and silicon photonic circuit in parallel as well as pre-testing the device/circuit performance. Furthermore, it ensures an efficient material usage. The GaSb photodiode has a cut-off wavelength at 2.45 μm, with a responsivity of 1.25 A/W, enabling various spectroscopic sensing applications. A μA level dark current is achieved under −0.3 V bias. These results demonstrate the potential of this platform for spectroscopic sensing in environmental monitoring, medical diagnostics, and industrial process control. The scalability of this integration approach makes it promising for large-scale, cost-effective SWIR photonic systems. Additionally, this photodiode can be co-integrated with on-chip tunable lasers at different wavelengths [20], enabling fully integrated spectroscopic sensing systems on a chip.

Acknowledgment. The authors would like to thank Dr. Yujie Guo and Dr. Chao Pang for the valuable discussion on photodiode measurements. Part of the work was supported by the France 2030 program (Equipex EXTRA, ANR-11-EQPX-0016).

Disclosures. The authors declare no conflicts of interest.

Data availability. Data underlying the results presented in this paper are not publicly available at this time but may be obtained from the authors upon reasonable request.

REFERENCES

1. A. Z. Subramanian, E. Ryckeboer, A. Dhakal, *et al.*, Photonics Res. **3**, B47 (2015).
2. R. Wang, A. Vasiliev, M. Muneeb, *et al.*, Sensors **17**, 1788 (2017).
3. E. Ryckeboer, A. Gassenq, M. Muneeb, *et al.*, Opt. Express **21**, 6101 (2013).
4. N. Hattasan, A. Gassenq, L. Cerutti, *et al.*, IEEE Photonics Technol. Lett. **23**, 1760 (2011).
5. A. Gassenq, N. Hattasan, L. Cerutti, *et al.*, Opt. Express **20**, 11665 (2012).
6. R. Wang, S. Sprengel, M. Muneeb, *et al.*, Opt. Express **23**, 26834 (2015).
7. R. Wang, M. Muneeb, S. Sprengel, *et al.*, Opt. Express **24**, 8480 (2016).
8. J. Long, P. Wang, H. Fang, *et al.*, Adv. Funct. Mater. **29**, 1803807 (2019).
9. Y. Guo, J. Han, D. Schaubroeck, *et al.*, *Graphene Week 2023* (2023).
10. C. Pang, Y. Deng, E. Kheradmand, *et al.*, APL Photonics **9**, 066113 (2024).
11. H. Lin, Y. Song, Y. Huang, *et al.*, Nat. Photonics **11**, 798 (2017).
12. S. Ghosh, R. Bansal, G. Sun, *et al.*, Sensors **22**, 3978 (2022).
13. C.-H. Liu, R. Bansal, C.-W. Wu, *et al.*, Adv. Photonics Res. **3**, 2100330 (2022).
14. J. Wu, Q. Jiang, S. Chen, *et al.*, ACS Photonics **3**, 749 (2016).
15. G. Roelkens, J. Zhang, L. Bogaert, *et al.*, APL Photonics **9**, 010901 (2024).
16. S. Cuyvers, A. Hermans, M. Kiewiet, *et al.*, Opt. Lett. **47**, 937 (2022).
17. D. Maes, S. Lemey, G. Roelkens, *et al.*, APL Photonics **8**, 016104 (2023).
18. J. Goyvaerts, S. Kumari, S. Uvin, *et al.*, Opt. Express **28**, 21275 (2020).
19. B. Kuyken, X. Liu, R. M. Osgood, *et al.*, Opt. Express **21**, 5931 (2013).
20. E. Soltanian, G. Muliuk, S. Uvin, *et al.*, Opt. Express **30**, 39329 (2022).

157.193.240.1 {ts '2024-12-18 08:54:16'}